https://doi.org/10.5194/acp-2020-1213
Preprint. Discussion started: 26 November 2020

Atmospheric Chemistry and Physics Discussions

Summer aerosol measurements over the East Antarctic seasonal ice zone.

Jack B. Simmons[1], Ruhi S. Humphries[2,3], Stephen R. Wilson[1], Scott D. Chambers[4], Alastair G. Williams[4], Alan D. Griffiths[4,1], Ian M. McRobert[5], Jason P. Ward[2], Melita D. Keywood,[2,3] Sean Gribben[2]

[1]Centre for Atmospheric Chemistry, School of Earth, Atmospheric and Life Sciences, University of Wollongong, Wollongong NSW 2522, Australia
[2]Climate Science Centre, CSIRO Oceans and Atmosphere, Aspendale VIC 3195, Australia
[3] Australian Antarctic Program Partnership, University of Tasmania, Hobart TAS, Australia
[4] ANSTO, Environmental Research, Locked Bag 2001, Kirrawee DC NSW 2232, Australia
[5] Engineering and Technology Program, CSIRO National Research Collections Australia, Hobart TAS 7004, Australia

Correspondence to: Jack Simmons (js828@uowmail.edu.au)

Abstract. Aerosol measurements over the Southern Ocean have been identified as critical to an improved understanding of aerosol-radiation and aerosol-cloud interactions, as there currently exists significant discrepancies between model results and measurements in this region. Previous springtime measurements from the East Antarctic seasonal ice zone revealed a significant increase in aerosol number concentrations when crossing the atmospheric polar front into the Polar cell. A return voyage in summer 2017 made a more extensive range of aerosols measurements, including in particular aerosol number concentrations and submicron size distributions. Again, significantly greater aerosol number concentrations were observed in the Polar cell than in the Ferrel cell. Unlike the previous spring voyage however, the polar front was unable to be identified by a step change in aerosol concentration. A possible explanation is that atmospheric mixing across the polar front occurs to a greater degree in summer, therefore weakening the atmospheric boundary at the front. This atmospheric mixing in summer complicates the determination of the polar front location. These changes, together with the increased source of precursors from phytoplankton emissions, are likely to explain the seasonal differences observed in the magnitude of aerosol populations between the Ferrel and Polar cell. In the present analysis, meteorological variables were used to identify different air-masses and then aerosol measurements were compared based on these identifications. CN_3 concentrations measured during wind directions indicative of Polar cell airmasses (median 594 cm^{-3}) were larger than those measured during wind directions indicative of Ferrel cell air (median 265 cm^{-3}). CN_3 and CCN concentrations were larger during periods where the absolute humidity was less than 4.3 g_{H2O}/m^3, indicative of free tropospheric or Antarctic continental airmasses, compared to other periods of the voyage. These results indicate that a persistently more concentrated aerosol population is present in the Polar cell over the East Antarctic seasonal ice zone, although the observed difference between the two cells may vary seasonally.

https://doi.org/10.5194/acp-2020-1213
Preprint. Discussion started: 26 November 2020

Atmospheric Chemistry and Physics Discussions

1 Introduction

Aerosol-radiation and aerosol-cloud interactions are among the most uncertain parameters in the current estimates of global radiative forcing (Myhre et al., 2013), and hence a major uncertainty in calculating the climate effects of changing atmospheric composition. This is true for both the uncertainty in future predictions as well as the modelling of past atmospheres. In particular, there is a need for reliable estimates of the pre-industrial atmosphere, as this is the reference-point for many calculations. Unlike greenhouse gases, the radiative impact of aerosols cannot be determined from atmospheric archives. However, measurements in pristine remote regions of the Earth can provide an insight into pre-industrial aerosol populations and processes (Carslaw et al., 2017), and have therefore been identified as critical to reducing this uncertainty (Carslaw et al., 2013). The Southern Ocean particularly has been identified as a pristine area of interest (Penner et al., 2012, Regayre et al., 2020).

Aerosol concentration, size distribution, and model parameters are poorly constrained over the Southern Ocean because of the sparsity of in situ aerosol measurements in the region. Longer-term in situ measurements have been made at terrestrial stations on the fringes of the Southern Ocean such as Cape Grim, Tasmania (40.7°S 144.7°E) (Gras and Keywood, 2017), Macquarie Island (54.5°S 158.9°E) (Brechtel et al., 1998), and Dumont D'Urville Station, Antarctica (66.7°S 140.0°E) (Legrand et al., 2016). Comparison between models and satellite measurements of aerosol (AOD) show significant underprediction of aerosol loading in this region (Shindell et al., 2013), suggesting a missing aerosol source in the far Southern Ocean and highlighting the need for further measurements. However, these satellite measurements are also poorly validated in this region due to the lack of in situ measurements.

There have also been numerous short-term ship-based aerosol measurement campaigns in the region. The first aerosol-focussed measurement campaign in the Southern Ocean occurred in 1995 during the first Aerosol Characterisation Experiment (ACE1). Ship based measurements taken between 41°S and 54°S observed a bimodal aerosol population dominated by sea salt (Quinn et al., 1998). A recent campaign of note was the Antarctic Circumnavigation Experiment's Study of Pre-Industrial-like Aerosols and Their Climate Effects (Schmale et al., 2019). They passed the longitudes considered here in their leg 1 at around 55°S.

The seasonal sea ice zone, the area of ocean between the permanent ice edge and winter sea ice maximum, covers a larger spatial area than the Antarctic continent itself. Previous measurements in this region are sparse. Davison et al. (1996) found maximum levels of DMS and methanesulfonic acid in aerosols in the seasonal sea ice region compared to open oceans further north. Other voyages have observed new particle formation events (Atkinson et al., 2012) and a previously unaccounted source of organic nitrogen in seasonal ice zone aerosol populations (Dall'Osto et al., 2017). These results suggest aerosol populations of the seasonal ice zones are distinct from those of the Antarctic continent and Southern Ocean.

Measurements from the East Antarctic seasonal ice zone are particularly scarce, though there is a growing body of research including measurements from this region. The first results from this region, from a 2012 campaign undertaken in the austral spring, known as SIPEX-II, produced surprising results: a step change increase in aerosol number concentration crossing the atmospheric polar front into the Polar cell (Humphries et al., 2016). The atmospheric polar front is the boundary between the Ferrel and Polar cells, the two major circulation cells impacting the Antarctic sea ice zone. Humphries et al.

https://doi.org/10.5194/acp-2020-1213
Preprint. Discussion started: 26 November 2020

Atmospheric Chemistry and Physics Discussions

(2016) identified the front using aerosol number concentration, which was then confirmed by meteorology data. A newly identified circulation mechanism that brought recently formed free-tropospheric secondary aerosols to the Polar cell surface was proposed to explain this observation, supported by extensive trajectory modelling. Given the magnitude of seasonal change experienced at high latitudes, it is not possible to extrapolate spring results to other seasons in this region. Observations made throughout the year are therefore important to fully develop understanding of this phenomenon. Here, in the summer season, we identify the polar front using a variety of variables and definitions to further understand the changes across this atmospheric boundary and use this to quantify the aerosol concentration and aerosol size distribution in the two air masses.

2 Methods

2.1 Measurement platform

Measurements were made aboard the *RV Investigator*, Australia's flagship blue-water research vessel managed by CSIRO's Marine National Facility, during the voyage IN2017_V01. The onboard atmospheric measurements (the Polar Cell Aerosol Nucleation project; PCAN) were a secondary objective of the voyage, the primary focus of which was mapping the bathymetry off the east Antarctic coast and retrieving sediment samples. The voyage departed Hobart, Australia on January 14, 2017. It tracked south-west for six days to the study area, south of 60° S and between 110° and 120° E, where the ship remained for 40 days. The ship returned to port on March 3, 2017 after a seven-day transit northeast. Within the survey area, the ship followed a 'mowing-the-lawn' pattern while seafloor mapping, resulting in high-resolution spatial coverage of a relatively small area. The ship was stationary, facing into the wind, for up to four hours at a time to allow for sediment retrieval. The voyage track, compared to that of the SIPEX-II voyage of 2012, is presented in Figure 1.

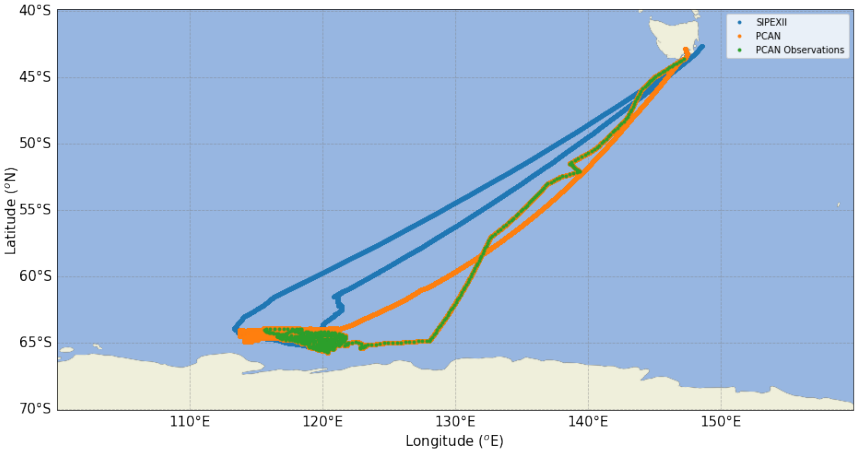

Figure 1: Voyage tracks of the SIPEX-II and PCAN voyages. Voyage tracks of the SIPEX-II (spring 2012, blue) and PCAN (summer 2017, orange) voyages overlap significantly, especially in the seasonal ice zone south of 60° S. This spatial overlap allows for seasonal comparison of measurements from the voyages. The green trace indicates the voyage period for which measurements were analysed. An interactive map of RV Investigator voyage tracks can be found here.

https://doi.org/10.5194/acp-2020-1213
Preprint. Discussion started: 26 November 2020


Atmospheric Chemistry and Physics Discussions

2.2 Measurements

Wind speed, direction and other meteorological parameters were measured from two locations (port and starboard) on a mast approximately 20 m above the Plimsoll line on the foredeck. This is approximately 25 metres above sea level. Meteorological measurements were made at 1 Hz resolution. Five-minute vector mean wind direction and mean wind speed values were calculated from the two meteorological stations and used for analysis.

Air for instrumental analysis was sampled from a stainless-steel inlet (internal diameter 150 mm), also located on the foredeck mast. Instruments were located in the aerosol laboratory, designed to be immediately below the mast in order to minimise the inlet length and thus aerosol sample losses. The flow rate through the inlet was approximately 420 LPM. Inlet losses have not yet been characterised for the aerosol sampling system aboard the *Investigator* but are a point of future work for the platform.

Number concentrations of in situ aerosols with diameter greater than 3 nm (CN_3) were measured using an ultrafine condensation particle counter (UCPC, TSI Model 3776, TSI, Shoreview, MN, USA). Measurements were made at 10 Hz temporal resolution, with 1 Hz averages output by the instrument. Air was sampled at 1.5 $Lmin^{-1}$ through the UCPC. Sample air for both aerosol number concentration and aerosol size distribution measurements were dried using a Nafion drier (Ecotech, Melbourne, VIC, Australia) in a bypass flow. Zeros (HEPA filtered outside air) and flow checks (external volumetric flowmeter) were made every second day during the voyage, with flow calibrations applied to the measurements in post-processing. A software malfunction led to incorrect times being assigned to measurements during the start of the voyage. This limited usable CN_3 measurements to the period from February 6th to the end of the voyage on March 4th.

Cloud condensation number concentration was measured using a Cloud Condensation Nuclei Counter (CCN100, Droplet Measurement Technologies, Longmont, Colorado, USA). CCN at 0.55% supersaturation ($CCN_{0.55}$) is reported in this study. Pressure corrections were applied to the data, collected at 1Hz and reported as five-minute means data. The sample flow was 0.5 $Lmin^{-1}$.

Aerosol size distributions (mobility diameter) were measured using a scanning mobility particle sizer (GRIMM nano Model 5.420 SMPS +C, Ainring, Bavaria, Germany). During PCAN particles between 8 and 500 nm were sized. Size distributions were measured at five-minute temporal resolution. Comparison to polystyrene latex spheres showed error in size classification of $\leq 5\%$ for particles of 81, 100 and 303 nm diameter.

^{222}Rn (radon) concentration was measured during the voyage using a 700 L dual-flow-loop two-filter radon detector, designed and built by the Australian Nuclear Science and Technology Organisation (Lucas Heights, NSW, Australia) (Chambers et al., 2014; Whittlestone and Zahorowski, 1998). Sampling occurred at 65-75 L min^{-1}. Calibration occurs on a quasi-monthly basis through radon injections from a Pylon (Ottawa, ON, Canada) ^{222}Rn source (20.62 ± 4% kBq ^{226}Ra).

Black carbon aerosol and CO_2 were also measured as part of the permanent instrumentation aboard the *RV Investigator*. Detailed descriptions of these measurements are available in Humphries et al. (2019). Significant periods of the voyage were affected by exhaust contamination of the sampled air due to the operational pattern of the ship. An automated exhaust removal procedure was used on the data using an algorithm designed by Humphries et al. (2019) which identifies and removes measurements when observations were highly variable or contaminated. Measurements of CN_3 and CO_2 that were greater

https://doi.org/10.5194/acp-2020-1213
Preprint. Discussion started: 26 November 2020


Atmospheric Chemistry and Physics Discussions

than the five-minute median added to three times the median absolute deviation; or containing black carbon concentrations greater than 0.07 ng m^{-3} were flagged as exhaust. Automatically filtered measurements were then manually inspected in conjunction with black carbon and CO_2 measurements for signs of contamination, and suspect periods removed. This was done in order to eliminate the influence of re-circulated, less concentrated exhaust.
To ensure comparability between the various quantities measured, this analysis has been limited to the time period of the shortest dataset, CN_3 measurements as noted above (February 6th until the end of the voyage).

2.3 Back trajectory modelling

Back trajectories presented were calculated using NOAA's HYbrid Single Particle Lagrangian Integrated Trajectory (HYSPLIT) model (Draxler and Hess, 1998). The ERA-Interim reanalysis dataset (European Centre for Medium-Range Weather Forecasts, 2019) was used to produce trajectories. The lack of meteorological observations at high latitudes means that there is significant uncertainty in the ERA-reanalysis dataset for polar regions which also applies to the trajectory products. Trajectories were calculated for each hour of the voyage and limited to 72 hours to minimize the accumulation of this uncertainty. Model vertical velocity was used to calculate vertical motion, and the end point was set at the ship's location at the end time at 20 m above sea level (approximately sampling height).

2.4 Data analysis

Data analysis was performed in the programming language 'R' (R Core Team, 2017). Code used for analysis and to produce figures included in this publication can be supplied upon request. All measurements used for analysis were resampled to five-minute time resolution. Confidence intervals for all reported values except in modal bin sizes were calculated in the style of McGill et al. (1978). Median concentrations are reported with 95% confidence intervals (denoted with CI) unless noted. Reported *r* values are Pearson correlation coefficients.

3 Results and Discussion

Previous research has used significant changes in the properties of local aerosol populations to identify the polar front. Humphries et al. (2016) observed a change in CN_3 and CN_{10} concentrations when crossing the polar front. No such step change was observed in the CN_3 measurements from the PCAN voyage, possibly because of the difference of seasons. Examination of other measurements including cloud condensation nuclei, radon and aerosol size distributions were also inconclusive when attempting to identify a boundary between the Ferrel and Polar cell. Instead, meteorological variables have been used to classify aerosol measurements. In the following sections, categorisation of air masses has been performed using both wind direction and absolute humidity. Following a definition of the borders of the categories, the aerosol properties within these categories are considered.

https://doi.org/10.5194/acp-2020-1213
Preprint. Discussion started: 26 November 2020

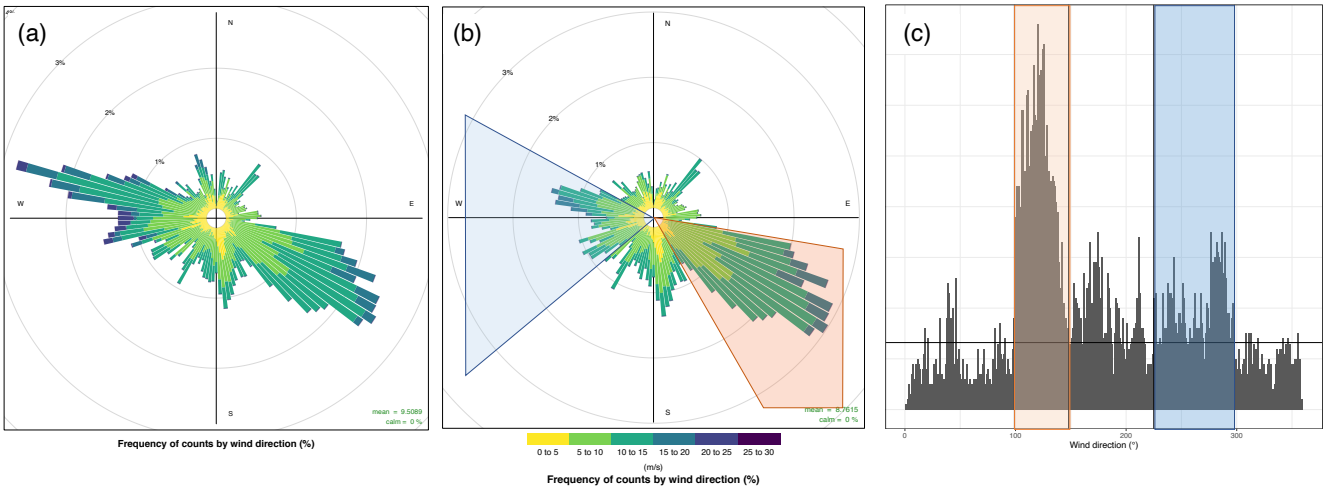

Figure 2: (a) Wind rose for the entire analysed PCAN voyage (February 6-March 4, 2017). (b) Wind rose for measurements south of 56.5° S, showing selected analysis. All wind measurements excluding the Transit category are plotted. There are two areas demonstrating a higher density of wind measurements, from the NW (Ferrel, sector: 225-298°, width 68°), and from the SE (Polar, sector 99-148°, width 49°). These sectors, capturing 52% of available wind measurements, are shaded in blue (Ferrel, 21%) and orange (Polar, 31%) respectively. (c) Frequency histogram of wind measurements plotted in 2b with 1° bin size. Ferrel (blue) and Polar (orange) sectors are highlighted.

3.1 Categorisation by wind direction

Wind direction was the first variable used to categorise measurements as it is central to the definitions of the Ferrel and Polar cells (Aguado and Burt, 2015). Figure 2a shows a wind rose of all analysed measurements (February 6th to March 4th). Fig. 2b shows a wind rose for the period of the analysed measurements as in Fig. 2a, however excluding the ship's transit back to Hobart. In this wind rose there are two areas of increased measurement density, showing the prevalence of both WNW and SE winds during the voyage. These areas agree with those expected from the three-cell model of atmospheric circulation. The southern edge of the Ferrel cell is expected to display a dominant NW wind, and the northern edge of the Polar cell is expected to be associated with a dominant SE wind.

The return transit to Hobart was dominated by strong winds from the NW (evidenced by the high density of measurements from this direction plotted in Fig. 2a), as expected in the open Southern Ocean at latitudes between the seasonal ice zone and southern Tasmania. The aerosol characteristics of these measurements differed from those observed in measurements made within the seasonal ice zone and were classified as "Transit" measurements. The boundary between Transit measurements and other categories was selected using wind speed and latitude. Measurements taken north of 56.5° S were classified as Transit and were associated with high wind speeds and extremely dominant westerly/north-westerly wind directions characteristic of the maritime environment in the open Southern Ocean. Transit measurements make up 15% of total measurements.

https://doi.org/10.5194/acp-2020-1213
Preprint. Discussion started: 26 November 2020


Atmospheric Chemistry and Physics Discussions

Measurements taken south of 56.5° S were then divided into one-degree wind direction bins and a frequency histogram plotted, presented in Fig. 2c. The frequency of wind measurements in each bin was used to create sectors attributable to the Ferrel cell (WNW) and Polar cell (SE). Bins which contained greater than 0.2% of total wind measurements encompassing the highest-density measurement regions were selected for analysis. Two windows were created, associated with the Ferrel cell (225-298°, 73° width, n = 1613) and the Polar cell (99-148°, 49° width, n = 2380). These sectors, shaded in Fig. 2b and c, contain 21% and 31% of total wind measurements, respectively. Wind direction was variable during the period of the voyage in which the ship was within the seasonal ice zone, indicating periods of influence from both the Ferrel cell and Polar cells. Measurements from the southerly sector (148-217°) have been excluded due to the potential influence of katabatic outflow on these measurements (Chambers et al., 2018). These southerly data are assumed to have been influenced chiefly by orographic factors and therefore any assumption regarding the air mass origin is difficult to make. Analysis of aerosol measurements from the southerly sector suggest influence from both Polar and Ferrel categories and have therefore been excluded. Boxplots of categorised CN_3 measurements are presented in the supplementary Figure S1. Wind measurements not classified as Ferrel, Polar or Transit were assigned "No category", and have been excluded from analysis.

A sensitivity analysis was performed on the Ferrel and Polar sectors and the results of this analysis are presented in the supplementary Table S1. Sectors were shifted 10° closer to 360°, 10° closer to 0°, symmetrically widened by 20° and symmetrically narrowed by 20°. The median CN_3 concentration of the selected Ferrel measurements is higher than or equal to each of the shifted Ferrel cell sectors, with all shifted sectors displaying median concentrations between 229 and 265 cm^{-3}. The selected Ferrel sector median CN_3 concentration is 265 (CI 252-279) cm^{-3}. Adjusting the Polar cell sector introduces more variability in median CN_3 concentration: adjusted sector concentrations range from 534-620 cm^{-3}. The median CN_3 concentration of the selected sector, 594 (CI 573-615) cm^{-3}, is in the upper region of this range. Thus, adjusting selection boundaries is expected to cause only small changes in the median particle concentration of the Ferrel and Polar cell sectors as a non-uniform particle source was being measured from a moving platform. The relatively small changes observed with shifted sectors demonstrates the median aerosol statistics reported are robust to boundary changes in selected wind sectors.

3.2 Categorisation by absolute humidity

Using measurements from the same voyage as discussed here, Chambers et al. (2018) found unexpected diurnal variability in radon concentrations during the voyage. Some periods displaying diurnal variability in radon were classified as katabatic outflow events. Events classed as katabatic outflow were associated with higher concentrations of CCN. A mid-morning radon minimum was especially indicative of this type of transport. Antarctic katabatic outflow air masses are often of free tropospheric origin (Chambers et al., 2018, Nylen et al., 2004) and are expected to be drier than those that have extended residence times over the local marine environment. Therefore, absolute humidity (AH) was the second meteorological variable used for categorising aerosol measurements. Categorisations were performed on the same set of measurements used for division by wind direction. Each categorisation

https://doi.org/10.5194/acp-2020-1213
Preprint. Discussion started: 26 November 2020

Atmospheric Chemistry and Physics Discussions

(whether by wind or AH) is therefore a subset of the total voyage measurement superset. Wind and AH categories overlap to differing degrees: a summary of overlaps is presented in Table S2
Absolute humidity was calculated using a derivation of the ideal gas law (Carnotcycle, 2012) from measured relative humidity and measured ambient temperature. A frequency histogram, presented in Figure 3, was constructed from the timeseries of AH measurements. Examining the distribution allowed three AH categories to be defined. These are defined in the first instance by a local minimum at 4.30 g_{H2O} m^{-3} in the frequency histogram of AH measurements. Measurements below this threshold were designated as Low AH. Measurements in the region 4.30-5.75 g_{H2O} m^{-3} were classified in the Mid AH category. Finally, measurements above 5.75 g_{H2O} m^{-3} were classed in the High AH category. 45% (n=3473) of valid AH measurements were classified as Low AH, 39% (n=3028) as Mid AH and 14% (n=1125) as High AH. The Low AH category is expected to capture air masses with either a katabatic flow or free-tropospheric source region as air from these sources have not had an extended residence time in a marine environment. The Mid AH is expected to consist largely of marine air masses. Note that the High AH category overlaps almost exclusively (>99%) with the Transit category determined by wind direction categorisation. This overlap is expected as the water saturation pressure is dependent on temperature. Ambient temperature increased during the transit from the Antarctic coast to Tasmania.

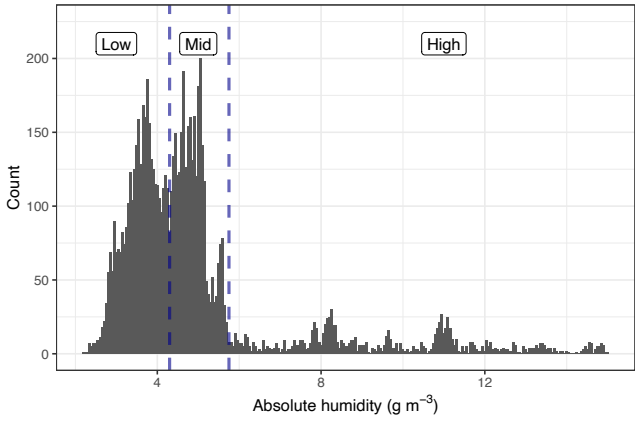

Figure 3: Frequency histogram of absolute humidity measurements including absolute humidity categories used for data analysis. The Low-Mid boundary is at 4.30 g_{H2O} m^{-3}, and the Mid-High boundary at 5.75 g_{H2O} m^{-3}.

3.3 Aerosol variables and radon grouped by wind direction

Figure 4 presents box plots of CN_3 (Fig. 4a), $CCN_{0.55}$ (Fig. 4b) and radon concentrations (Fig. 4c) grouped by wind direction. In each case the median concentration is higher in Polar cell measurements than in Ferrel cell measurements. Median CN_3 concentration in the Polar cell, 594 (CI 573-615) cm^{-3} is approximately a factor of two larger than the Ferrel cell median, at 263 (250-277) cm^{-3}. Median $CCN_{0.55}$ concentrations in the Polar cell were 208 (CI 176-240) cm^{-3}, compared to a median concentration of 113 (CI 84-142) cm^{-3} in the Ferrel cell. Median radon concentration in the Polar cell was 78.3 (CI 73.3-83.3) mBq m^{-3} compared to 59.1 (CI 54.3-63.9) mBq m^{-3} in the Ferrel cell. For both aerosol variables the transit category median is between those observed in the Polar and Ferrel, evident when examining Fig. 4. This is likely because of the mix of marine and continental sources further north

https://doi.org/10.5194/acp-2020-1213
Preprint. Discussion started: 26 November 2020


Atmospheric Chemistry and Physics Discussions

rather than being a mix of Ferrel and Polar air masses. Figure data are also presented in tabular form in supplementary Table S2.

Median aerosol size distributions divided by wind category are presented in Figure 5a. Each category displays a bimodal distribution. The Transit distribution is the most strongly bimodal. This is indicative of heavily cloud-processed marine aerosol (Hoppel et al., 1990) and results in one modal maximum in the Aitken mode (37.2 nm) and the other in the accumulation mode (157 nm). The median magnitude of the modes are 421 (CI 378-464) and 288 (CI 251-326) cm^{-3} respectively.

In contrast, the distributions plotted for the Ferrel and Polar cells differ from the Transit period distribution. Both Polar and Ferrel distributions contain two local maxima with a smaller degree of bimodality. It should be noted that all aerosol populations, even those potentially descending from the free troposphere, had the potential to be cloud processed before sampling. Thus, observed bimodality in all categories is not surprising. The Polar airmass has a higher particle concentration across the distribution than the Ferrel (as expected accounting for the larger median CN_3 concentration). The difference is relatively uniform across the distribution between 20 and 120 nm. The Polar and Ferrel distributions have modes in similar size ranges: the smaller mode in the Polar cell has a maximum at 38.5 nm, and at 40 nm in the Ferrel. The larger mode is at a slightly larger diameter in the Ferrel cell dataset (109 nm) than the Polar cell (101 nm). Modal sizes and concentrations from Fig. 5 are summarised in the supplementary Table S3. This finding has been observed previously in the east Antarctic seasonal ice zone. In addition to the spring 2012 campaign SIPEXII (Humphries et al., 2016) and identification of katabatic influence on local CCN concentration (Chambers et al., 2018) referred to previously, there is evidence for a change in aerosol population across the polar front during a summer latitudinal transect of the Southern Ocean in 2016 (Alroe et al., 2019), along with variability in the Aitken mode dependant on marine biological precursors and synoptic scale systems.

Modal size bins in median distributions are retrieved directly from the median distributions: that is the bin with highest median concentration in the Aitken and accumulation size range is reported as the mode. To estimate uncertainty in the modal particle size for Aitken and accumulation mode aerosol, the bin with maximum concentration was retrieved from each individual distribution and analysed. Details of this analysis are found in the supplementary information S1. These results, summarised in the supplementary Table S4, are different to the modal bin sizes retrieved for the overall median distributions noted above. This is expected as the modal size bin is dependent of the concentration in the bin. The Aitken mode in the Polar cell, located at 35.9 (CI 34.5-36.7) nm, is significantly smaller than the corresponding mode in the Ferrel cell, at 40.0 (CI 38.5-41.6) nm. The accumulation mode in the Polar measurements at 98.2 (CI 94.9-101) nm is also significantly smaller than that in the Ferrel measurements at 109 (CI 106-116) nm. The median mode of individual distributions are plotted with 95% CI are plotted for each category in Fig. 5.

https://doi.org/10.5194/acp-2020-1213
Preprint. Discussion started: 26 November 2020

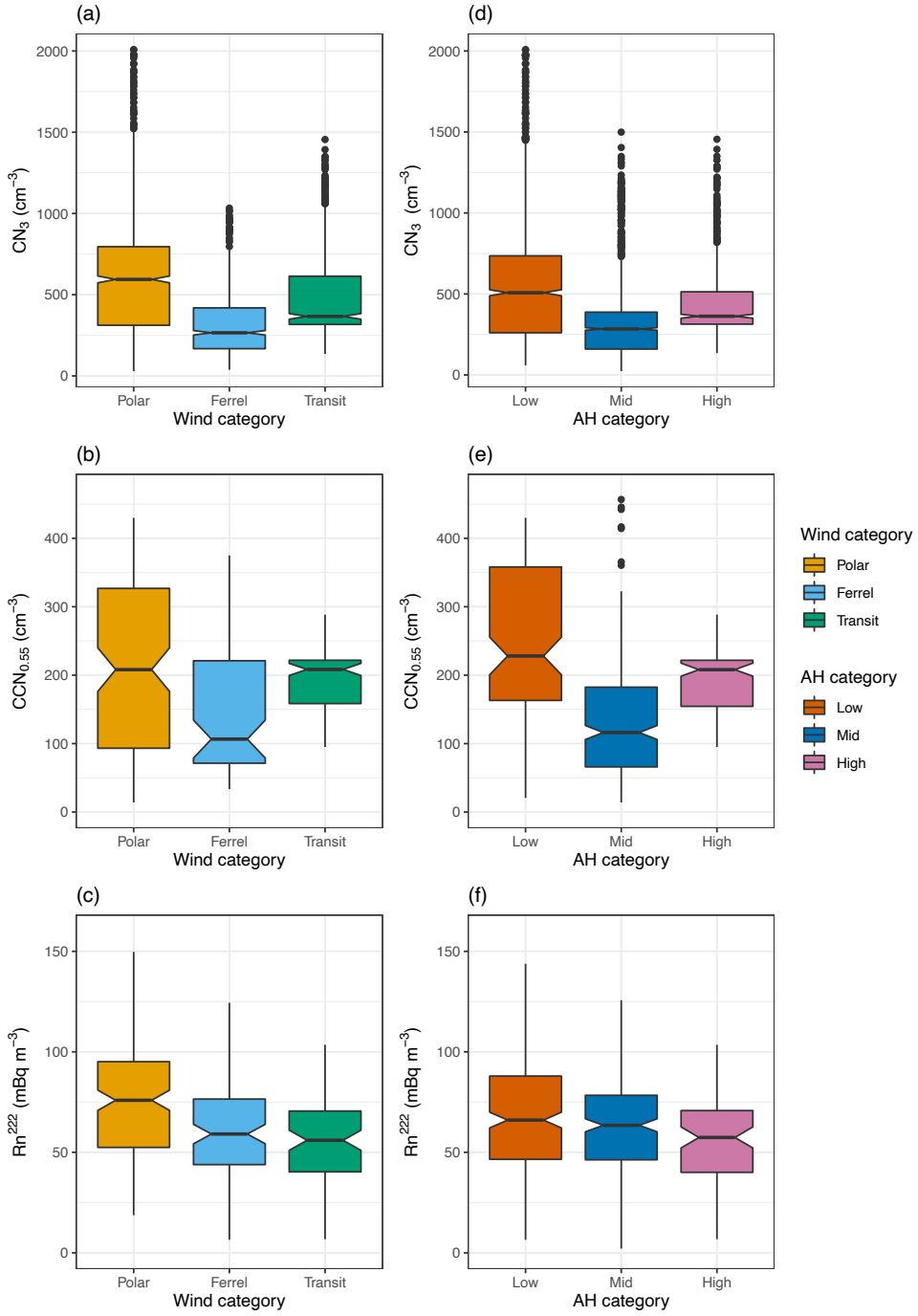

310 **Figure 4: Box plots divided by category for (a) and (d) CN_3, (b) and (e) $CCN_{0.55}$, and (c) and (f) Rn^{222}. Plots in the left-hand column are split by wind category and plots in the right-hand column are split by absolute humidity. Notches indicate the 95% confidence intervals in the median. Black dots represent outliers, defined as points greater than 1.5 times the interquartile ranges distant from the nearest quartile. Medians and confidence intervals for each variable in each category are reported in the supplementary Table S3. Outliers have been excluded from (c) and (f) to allow better representation of concentration differences.**

315

https://doi.org/10.5194/acp-2020-1213
Preprint. Discussion started: 26 November 2020

Atmospheric Chemistry and Physics Discussions

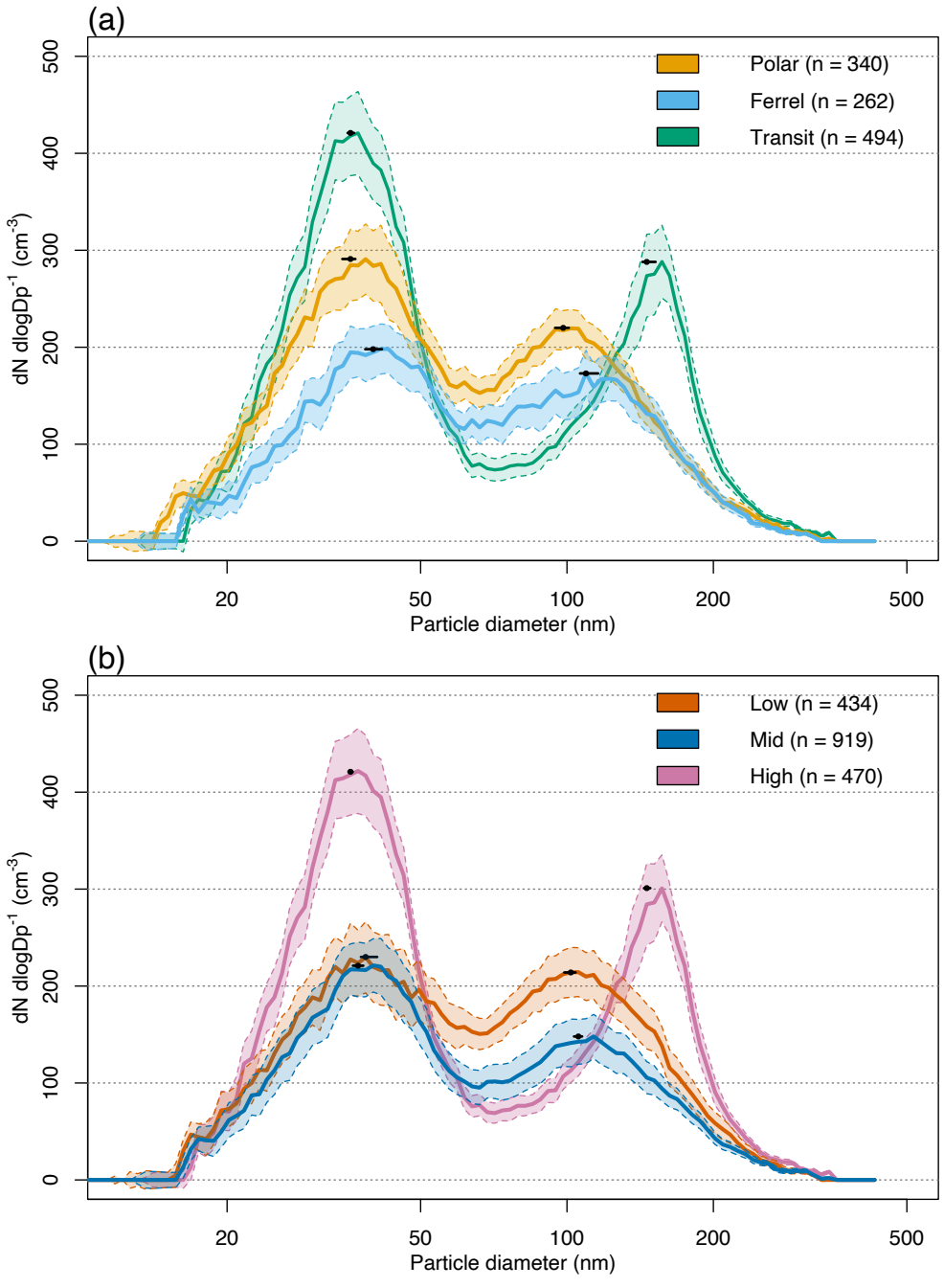

Figure 5: Median particle size distributions for (a) each wind category and (b) each AH category. Shaded areas represent the 95% confidence interval in the median for each bin size. The modal sizes and concentrations for each distribution are reported in the supplementary Table S3. Black points plotted on each distribution indicates the median Aitken and accumulation mode generated from analysis of individual size distributions. Error bars represent at 95% confidence interval. More detail is provided in the supplementary information S1, and Table S4.

https://doi.org/10.5194/acp-2020-1213
Preprint. Discussion started: 26 November 2020


Atmospheric Chemistry and Physics Discussions

3.4 Aerosol variables and radon grouped by absolute humidity

Fig. 4 also displays boxplots of CN_3, $CCN_{0.55}$ and radon concentrations grouped by absolute humidity category. Measurements of CN_3 and $CCN_{0.55}$ in the Low AH category are higher than those in the Mid and High AH categories. Median CN3 and $CCN_{0.55}$ concentrations in the Low AH category were 507 (CI 489-526) cm^{-3} and 228 (CI 201-255) cm^{-3} respectively. In comparison, the Mid AH medians for CN_3 and $CCN_{0.55}$ were 284 (CI 276-292) cm^{-3} and 117 (CI 107-128) cm^{-3}, respectively. This agrees with the finding that katabatic outflow events are associated with higher aerosol concentrations than locally sampled air masses observed by Chambers et al. (2018), as katabatic outflow events are likely included in the Low AH category. While small, a difference in radon concentration is also noted between the categories: a median of 68.1 (CI 64.0-72.1) mBq m^{-3} in during Low AH compared to 63.6 (CI 60.3-66.9) mBq m^{-3} during Mid AH. It is likely that the Low AH category captures the katabatic outflow present in Type 3 and Type 4 days presented in Chambers et al. (2018). The median $CCN_{0.55}$ concentration observed in the present analysis for Low AH agrees well with maximum CCN concentrations reported for mid-morning katabatic outflow CCN peaks (Chambers et al., 2018). It should be noted that the Low AH category includes a greater percentage of the measurements (45%) compared to the Type 3 and 4 days reported by Chambers et al. (2018) (~27%) so likely includes measurements not influenced by katabatic drainage.

Median size distributions plotted for each AH category are presented in Fig. 5b. Unsurprisingly, the High AH category overlapped significantly with the Transit category, a measurement of open ocean Ferrel cell aerosol. Similar to Fig. 5a, each distribution shows bimodal character. The Low AH and Mid AH have a smaller magnitude of bimodality. The smaller mode in each of these distributions, in the Aitken range, is similar in magnitude and concentration: at 38.5 nm with concentrations of 230 (CI 193-266) cm^{-3} in Low AH and at 40.0 nm, concentration 221 (CI 194-249) cm^{-3} in Mid AH. The larger mode is more concentrated in the Low AH category, with a concentration of 214 (CI 189-240) cm^{-3} at 106 nm, than the Mid AH: concentration 148 (CI 125-171) cm^{-3} at 113 nm.

Analysis of the median modes from individual distributions, as with wind categorisation, reveals slight differences to the modes retrieved from the overall median distribution. The Low AH category has an Aitken mode at 37.6 (CI 36.6-38.6) nm. This mode is located at 35.9 (CI 35.2-36.6) nm in the Mid AH category. The accumulation modes are also different: 103 (CI 101-105) nm in the Low AH category compared to 108 (CI 106-110) nm in the Mid AH category.

3.5 Evidence for large-scale atmospheric transport influence on SO aerosol populations

Although an instantaneous change in observed aerosol populations attributable to crossing of the Polar Front was not observed during PCAN as it was during SIPEXII, large differences in CN_3 and $CCN_{0.55}$ concentration become evident when meteorological variables are used to group aerosol measurements. Grouping measurements by wind direction produces higher median concentrations of CN_3 and CCN sampled during wind directions indicative of Polar cell air. Similarly, higher concentrations of CN_3 and

https://doi.org/10.5194/acp-2020-1213
Preprint. Discussion started: 26 November 2020


Atmospheric Chemistry and Physics Discussions

$CCN_{0.55}$ were observed when AH is less than 4.3 g_{H2O}/m^3. The southerly flow of Polar cell air is expected to be drier than Ferrel cell air (which has a theoretically longer residence time in the marine boundary layer as well as having increased contact with warmer ocean water, compared to contact with cold continent and sea ice expected for Polar cell air). These results provide evidence that large-scale atmospheric transport (i.e. the atmospheric transport included in the Polar and Ferrel cells) influences local aerosol populations in the east Antarctic seasonal ice zone. Note, however, that the aerosol populations sampled under different wind and AH regimes are not entirely distinct. Aerosol size distributions are similar between Polar and Ferrel wind measurements, and between Low and Mid AH categories. The similarity between Polar and Ferrel median size distributions pictured in Fig. 5 indicates that a common aerosol source may contribute to these populations. The difference (smaller particle concentrations in the Ferrel cell, along with slightly larger modal sizes) suggest the Ferrel cell population may be a product of an aging Polar cell population. This is supported by the inference that Ferrel cell aerosol populations have spent a longer time in the marine boundary layer, providing more opportunity for coagulation and condensation.

Back trajectory analysis can be used to further identify influence of large-scale atmospheric processes on boundary layer aerosol in the east Antarctic seasonal ice zone. HYSPLIT back trajectories were run for each hour, on the hour, of the voyage. The ship's location at each time was used as the trajectory end point. Trajectories were separated into wind and absolute humidity categories using a similar method to that used for the aerosol measurements. The classification category for the wind direction or AH at the trajectory endpoint was used to classify the trajectory. Median vertical profiles, frequency histograms and trajectory maps for each category were constructed, presented in the supplementary Figures S2 and S3.

Distinct air mass histories are expected to contribute to different aerosol population characteristics observed in each classification. Back trajectory analysis suggests a greater free tropospheric influence is present in the Polar wind category compared to the Ferrel wind category. The boundary layer height in this region of the Southern Ocean has been measured to be 900±400 m north of the polar front and 700±200 m south of the polar front during summer and early autumn voyages (Alexander and Protat, 2019). The median profile for the Polar category shows air masses residing above 1000 m.a.g.l. 48 hours before the trajectory endpoint. Sampled air masses in the Polar category are therefore likely to have significant free-tropospheric influence. The median profiles for the Ferrel and Transit wind categories show no such development, instead keeping close to the surface for the duration of the 72 hours modelled (Fig. S2). The large interquartile ranges on this plot reflect significant variability in airmass altitude.

A similar result is generated when examining trajectories grouped by AH category. The Mid and High AH category median trajectory vertical profiles show little vertical development in the 72 hours prior to measurement (Fig. S3). In contrast, the Low AH category median vertical profile demonstrates vertical development comparable to that of the Polar wind category with significant residence time at free tropospheric altitudes in the 72 hours prior to sampling.

Back trajectories indicate a greater free tropospheric influence on airmasses sampled under Polar wind regimes and with low AH than during other measurement periods. Higher particle counts (CN_3 and CCN) are also observed in these air masses. Observation of higher aerosol number concentrations and a free tropospheric influence on air masses sampled in the Polar cell in the east Antarctic seasonal ice

https://doi.org/10.5194/acp-2020-1213
Preprint. Discussion started: 26 November 2020


Atmospheric Chemistry and Physics Discussions

zone are common to the summer measurements presented here and the spring measurements reported in Humphries et al. (2016). However, there are some key differences between measurements suggesting different source and air mass transport mechanisms.

3.6 Evidence for seasonality in seasonal ice zone regional aerosol sources

Comparing SIPEXII Polar cell aerosol measurements from spring 2012 to the PCAN Polar measurements (classified by wind direction) indicates there may be different sources, or source strengths, for populations between spring and summer despite some similar characteristics. The median CN_3 concentration in the Polar cell during SIPEXII was 816 cm^{-3} (Humphries et al., 2016), compared to a median Polar CN_3 concentration of 594 cm^{-3} reported here. The median SIPEXII Ferrel cell concentration was 196 cm^{-3}, compared to a median of 263 cm^{-3} during PCAN. The magnitude of the change between the Polar and Ferrel cell during SIPEXII was a factor of approximately four whereas for PCAN this change is closer to a factor of two.

A further difference between spring and summer measurements becomes evident when considering the size of particle populations measured during the voyages. The Ferrel-Polar cell transition during SIPEXII was especially prominent in the $CN_{3\text{-}10}$ fraction. This is attributed to a change of aerosol source by Humphries et al. (2016). A lack of a CN_{10} measurement on board during PCAN (due to instrument malfunctions) prevents a direct comparison of this metric between voyages. Aerosol size distribution measurements from PCAN can be used however: the SMPS instrument used on this voyage observed measurements as small as 8 nm diameter during the voyage, in the $CN_{3\text{-}10}$ range. Distributions for Polar and Ferrel measurements during PCAN presented in Fig. 5a are very similar at the small end of the size range measured. This suggests the difference in aerosol number concentration observed during PCAN is not driven by a large change in concentration of very small particles as observed during SIPEXII.

Polar cell measurements from SIPEXII and PCAN (defined by wind direction) were compared to investigate this idea further. Figure 6 displays four correlation plots: AH measurements and atmospheric pressure measurements from PCAN (top row) and SIPEXII (bottom row) are plotted against CN_3 measurements. Events of anomalously high CN_3 concentration during SIPEXII as identified by Humphries et al. (2015) are excluded from this analysis. CN_3 shows a negative relationship with absolute humidity in PCAN Polar cell measurements (r = -0.50). This relationship is weaker for SIPEXII measurements (r = -0.26). Instead, a negative relationship is observed between SIPEXII Polar cell CN_3 measurements and atmospheric pressure (r = -0.61), discussed in detail in Humphries et al. (2016). This relationship is weaker in the PCAN Polar cell measurements (r = -0.23). This suggests the source regions or mechanisms of measured Polar cell aerosol in the east Antarctic seasonal ice zone may vary between seasons. A free tropospheric injection model presented by Humphries et al. (2016), assosciated with events of local low atmospheric pressure, was used to account for unexpectedly high concentrations of small aerosol during SIPEXII. This tropospheric injection may not be the dominant source of Polar cell aerosol measured during summer 2017. This conclusion was also drawn from the analysis of radon diurnal cycles and CCN concentrations from the PCAN voyage (Chambers et al., 2018), which highlighted the contribution of katabatic outflow to the aerosol populations of the near-shore atmosphere of the east Antarctic.

https://doi.org/10.5194/acp-2020-1213
Preprint. Discussion started: 26 November 2020

Atmospheric Chemistry and Physics Discussions

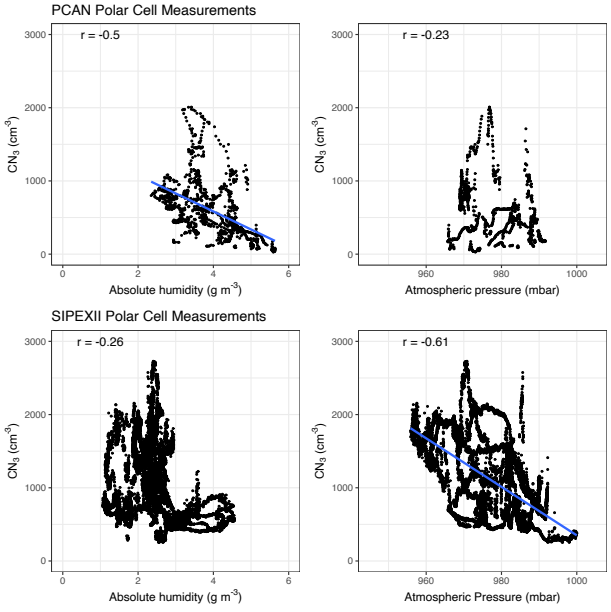

Figure 6: Comparison of PCAN (top row) and SIPEXII (bottom row) AH and pressure measurements plotted against CN_3 measurements in the Polar cell. Linear regression lines are plotted on the stronger relationship for each voyage. Pearson's *r* values are plotted on each facet.

3.7 Explaining the observed seasonality

Higher concentrations of aerosol number concentration (expressed as CN_3, CN_{10} or CCN) are observed in the Polar cell influenced airmasses in the east Antarctic seasonal ice zone during both spring and summer compared with Ferrel cell airmasses. However, the magnitude of this change is different between seasons. Though a direct comparison cannot be made, size-resolved measurements suggest different size distributions between voyages could be expected. Therefore, it seems different source and transport mechanisms may influence Polar cell aerosol populations in the seasonal ice zone in spring and summer.

During spring, the circumpolar trough (an alternative name for the polar front), the region of low pressure surrounding the Antarctic continent, is at peak intensity and located closest to the Antarctic coast (Pook, 2002). This serves to strengthen westerly winds in the southern Ferrel cell and intensify the pressure gradient across the trough. This may be associated with limited atmospheric transport across the polar front. This could cause the Polar and Ferrel cells to be more isolated from each other, creating a 'boundary' observable in aerosol populations. Stronger low-pressure systems are present in the region in spring (evidenced by the lower atmospheric pressures measured during SIPEXII compared to PCAN, Fig. 6) compared to summer. These strong low-pressure events inject CN_3 into the Polar cell boundary layer from the free troposphere (Humphries et al., 2016) causing the correlation between atmospheric pressure and CN_3 concentration observed in the SIPEXII measurements.

https://doi.org/10.5194/acp-2020-1213
Preprint. Discussion started: 26 November 2020


Atmospheric Chemistry and Physics Discussions

The circumpolar trough weakens in summer (Pook, 2002). This may allow more inter-cell atmospheric transport between the Polar and Ferrel cells. A lack of clear 'boundary' observable in aerosol populations in PCAN measurements between the cells could be symptomatic of this, as are similar median aerosol size distributions for measurements classified as Polar cell and Ferrel cell. Low pressure systems in the region are generally weaker in summer, and therefore the free tropospheric injection of small particles could be less dominant in the Polar cell. This explains the weaker relationship between CN_3 and atmospheric pressure in PCAN Polar cell measurements. Instead, the katabatic outflow influencing the measurements in the Polar cell documented by Chambers et al. (2018) becomes dominant and strengthens the relationship between CN_3 concentration and AH. It must also be considered that differences in tropospheric radon at coastal Antarctic stations between summer and winter provide evidence for seasonality in recent terrestrial influence on the remote Southern Ocean boundary layer (Chambers et al.,2018).

It is clearly possible, however, to have periods in any season with strong low-pressure systems and so this hypothesis requires testing over varying meteorological conditions. Results from a more recent summer voyage do observe distinct changes in aerosol properties (Humphries et al., in prep.), demonstrating the complexity of the region.

A further difference between the seasons is the strength of aerosol sources. Phytoplankton blooms are known to occur around Antarctica in late spring and summer which can act as an additional particle source via the production of aerosol precursor gases (Charlson et al., 1987). Increased organic fractions in summer Antarctic aerosol observations provide evidence for this mechanism (Hong et al., 2020). Concentrations of biogenic aerosol precursors are particularly high during periods of sea ice melt in the spring (Yan et al., 2020; Gabric et al., 2018) which may contribute to increased SOA formation during this period. The magnitude of the algal bloom is greatest in the waters off the west Antarctic Peninsula, but does still occur in the East Antarctic (Deppeler and Davidson, 2017). The influence of phytoplankton blooms on ultrafine aerosol has been observed in this region before. Alroe et al. (2017) measured enhancements in Aitken and nucleation mode aerosol in the Southern Ocean off east Antarctica associated with air mass back trajectories passing over biologically productive regions. The annual cycle of this particle precursor source must therefore be considered when examining aerosol populations of the region.

4 Conclusions

There is no definitive transition in aerosol properties across the polar front evident in summer 2017 measurements from the east Antarctic seasonal ice zone. Dividing aerosol measurements by meteorological variables however assists in interpreting the dataset. Local winds from the SE, indicative of Polar cell air masses, displayed median CN_3 and $CCN_{0.55}$ concentrations much greater than when local wind direction was from the NW (indicative of Ferrel cell air masses). The magnitude of this difference is smaller in the present measurements than observed between Polar and Ferrel cells during spring 2012. Similarly, aerosol measurements taken during periods where absolute humidity was less than $4.3 g_{H2O} m^{-3}$ were also associated with enhancements in CN_3 and CCN number concentration compared to other periods of the voyage.

https://doi.org/10.5194/acp-2020-1213
Preprint. Discussion started: 26 November 2020


Atmospheric Chemistry and Physics Discussions

These results indicate that large-scale atmospheric transport mechanisms may influence aerosol populations in the east Antarctic seasonal ice zone. Evidence of seasonality of aerosol measurements in the Polar cell also emerges when comparing summer to spring measurements. Differing relationships between CN_3, atmospheric pressure and absolute humidity indicate that sampled aerosol populations may have modified source regions or mechanisms.

Seasonal differences in aerosol populations observed in the East Antarctic seasonal ice zone may be explained using the following conceptual model. The distinct boundary in atmospheric composition observed during spring measurements may be a result of a strengthened circumpolar trough (Pook, 2002), isolating the airmasses of the Ferrel and Polar Cells. Polar cell aerosol populations are driven by tropospheric injection of ultrafine particles into the boundary later, as suggested by Humphries et al. (2016). In contrast, the summer in this region generally exhibits a weakened circumpolar trough. This weakening would allow a greater air mass transfer between the Ferrel and Polar cells, and weaken the atmospheric boundary defined by sampled aerosol population. The reduction in strength of the Ferrel cell-Polar cell atmospheric boundary could reduce the difference between the two airmasses' aerosol populations. Synoptic low-pressure systems could be expected to occasionally inject ultrafine particles from the free troposphere into the marine boundary layer. This may occur more frequently in spring due to more frequent, stronger synoptic systems. This case is not observed in the present measurements. Instead, the dominant source of particle number enhancement is katabatic outflow from the Antarctic continent.

This work provides evidence for a seasonal cycle of aerosols in the east Antarctic seasonal ice zone, and further strengthens the free tropospheric transport mechanism proposed by Humphries et al. (2016). Measurements of air mass movements on the meso scale such as a wind profiling boundary layer radar would also be of use in seeking to confirm source regions of sampled aerosol populations and distinguishing air mass movements on a scale finer than that detected by models. Greater understanding could be gained from measurement campaigns with durations longer than the synoptic timescale as the discussed process have influence on a regional, rather than local, spatial scale. Increased density of aerosol observations throughout the year, including additional campaigns in summer and spring would also assist in understanding the complex factors driving aerosol populations in the troposphere of the East Antarctic seasonal ice zone.

5 Code and data Availability

Software code in the language 'R' used in generating the present manuscript is available from the corresponding author upon request. All data and samples acquired on the voyage are made publicly available in accordance with MNF Policy. Measurements are available through the CSIRO Data Access Portal.

6 Author contribution

RH instigated the PCAN investigation, along with JW and MK, and coordinated deployment. JS was responsible for on-board data collection, data analysis and manuscript preparation. RH and SRW

https://doi.org/10.5194/acp-2020-1213
Preprint. Discussion started: 26 November 2020

provided scientific advice, data analysis expertise and manuscript preparation guidance. SC, AG and AW installed and maintain the radon monitor on board the *RV Investigator*. IR was responsible for the installation of many aerosol instruments on the *Investigator.* SG ran the offline HYSPLIT model. All authors contributed to reviews of the manuscript.

7 Competing interests

The authors declare that they have no conflict of interest.

8 Acknowledgements

The authors gratefully acknowledge Dr. Leanne Armand, Chief Scientist on board voyage IN2017-V01, and other voyage staff for allowing the PCAN piggyback project on board the *RV Investigator*. The Authors wish to thank the CSIRO Marine National Facility (MNF) for its support in the form of sea time on *RV Investigator*, support personnel, scientific equipment and data management with particular thanks to the Seagoing Instrumentation Team. In particular we thank the technical and IT support personnel on board the voyage. All data and samples acquired on the voyage are made publicly available in accordance with MNF Policy. This project received grant funding from the Australian Government as part of the Antarctic Science Collaboration Initiative program. The Australian Antarctic Program Partnership is led by the University of Tasmania, and includes the Australian Antarctic Division, CSIRO Oceans and Atmosphere, Geoscience Australia, the Bureau of Meteorology, the Tasmanian State Government and Australia's Integrated Marine Observing System.

https://doi.org/10.5194/acp-2020-1213
Preprint. Discussion started: 26 November 2020

Atmospheric Chemistry and Physics Discussions

References

Aguado, E., and Burt, J.E.: Atmospheric Circulation and Pressure Distributions, in *Understanding Weather and Climate*, Pearson, London, UK , 2015.

Alexander, S. P., and Protat, A.: Vertical Profiling of Aerosols With a Combined Raman-Elastic Backscatter Lidar in the Remote Southern Ocean Marine Boundary Layer (43–66°S, 132–150°E), J. Geophys. Res.-Atmos., 124, 12107-12125, 10.1029/2019jd030628, 2019.

Alroe, J., Cravigan, L. T., Miljevic, B., Johnson, G. R., Selleck, P., Humphries, R. S., Keywood, M. D., Chambers, S. D., Williams, A. G., and Ristovski, Z. D.: Marine productivity and synoptic meteorology drive summer-time variability in Southern Ocean aerosols, Atmos. Chem. Phys. Discuss., 2019, 1-27, 10.5194/acp-2019-1081, 2019.

Atkinson, H. M., Huang, R. J., Chance, R., Roscoe, H. K., Hughes, C., Davison, B., Schönhardt, A., Mahajan, A. S., Saiz-Lopez, A., Hoffmann, T., and Liss, P. S.: Iodine emissions from the sea ice of the Weddell Sea, Atmos. Chem. Phys., 12, 11229-11244, 10.5194/acp-12-11229-2012, 2012.

Brechtel, F. J., Kreidenweis, S. M., and Swan, H. B.: Air mass characteristics, aerosol particle number concentrations, and number size distributions at Macquarie Island during the First Aerosol Characterization Experiment (ACE 1), J. Geophys. Res.-Atmos., 103, 16351-16367, doi:10.1029/97JD03014, 1998.

How to convert relative humidity to absolute humidity: https://carnotcycle.wordpress.com/2012/08/04/how-to-convert-relative-humidity-to-absolute-humidity/, last access: July 7, 2020.

Carslaw, K. S., Lee, L. A., Reddington, C. L., Pringle, K. J., Rap, A., Forster, P. M., Mann, G. W., Spracklen, D. V., Woodhouse, M. T., Regayre, L. A., and Pierce, J. R.: Large contribution of natural aerosols to uncertainty in indirect forcing, Nature, 503, 67-71, 10.1038/nature12674, 2013.

Carslaw, K. S., Gordon, H., Hamilton, D. S., Johnson, J. S., Regayre, L. A., Yoshioka, M., and Pringle, K. J.: Aerosols in the Pre-industrial Atmosphere, Current Climate Change Reports, 3, 1-15, 10.1007/s40641-017-0061-2, 2017.

Chambers, S. D., Preunkert, S., Weller, R., Hong, S.-B., Humphries, R. S., Tositti, L., Angot, H., Legrand, M., Williams, A. G., Griffiths, A. D., Crawford, J., Simmons, J., Choi, T. J., Krummel, P. B., Molloy, S., Loh, Z., Galbally, I., Wilson, S., Magand, O., Sprovieri, F., Pirrone, N., and Dommergue, A.: Characterizing Atmospheric Transport Pathways to Antarctica and the Remote Southern Ocean Using Radon-222, Front. Earth Sci., 6, 10.3389/feart.2018.00190, 2018.

Chambers, S. D. H., S.-B.; Williams, A. G.; Crawford, J.; Griffiths, A. D.; Park, S.-J.: Characterising terrestrial influences on Antarctic air masses using Radon-222 measurements at King George Island, Atmos. Chem. Phys., 14, 9903-9916, 10.5194/acp-14-9903-2014, 2014.

Charlson, R. J., Lovelock, J. E., Andreae, M. O., and Warren, S. G.: Oceanic phytoplankton, atmospheric sulphur, cloud albedo and climate, Nature, 326, 655-661, 10.1038/326655a0, 1987.

Dall'Osto, M., Ovadnevaite, J., Paglione, M., Beddows, D. C. S., Ceburnis, D., Cree, C., Cortés, P., Zamanillo, M., Nunes, S. O., Pérez, G. L., Ortega-Retuerta, E., Emelianov, M., Vaqué, D., Marrasé, C., Estrada, M., Sala, M. M., Vidal, M., Fitzsimons, M. F., Beale, R., Airs, R., Rinaldi, M., Decesari, S., Cristina Facchini, M., Harrison, R. M., O'Dowd, C., and Simó, R.: Antarctic sea ice region as a source of biogenic organic nitrogen in aerosols, Sci. Rep. UK, 7, 6047, 10.1038/s41598-017-06188-x, 2017.

Davison, B., O'Dowd, C., Hewitt, C. N., Smith, M. H., Harrison, R. M., Peel, D. A., Wolf, E., Mulvaney, R., Schwikowski, M., and Baltensperger, U.: Dimethyl sulfide and its oxidation products in the atmosphere of the Atlantic and southern oceans, Atmos. Environ., 30, 1895-1906, 10.1016/1352-2310(95)00428-9, 1996.

Deppeler, S. L., and Davidson, A. T.: Southern Ocean Phytoplankton in a Changing Climate, Frontiers in Marine Science, 4, 10.3389/fmars.2017.00040, 2017.

Draxler, R. R., and Hess, G. D.: An overview of the HYSPLIT_4 modelling system for trajectories, dispersion and deposition, Aust. Meteorol. Mag., 47, 295-308, 1998.

ERA-Interim: https://www.ecmwf.int/en/forecasts/datasets/reanalysis-datasets/era-interim, access: March 25, 2019.

Gabric, A., P. Matrai, G. Jones, and J. Middleton (2018), The Nexus between Sea Ice and Polar Emissions of Marine Biogenic Aerosols, B. Am. Meteorol. Soc., 99(1), 61-81, doi: 10.1175/bams-d-16-0254.1.

Gras, J. L., and Keywood, M.: Cloud condensation nuclei over the Southern Ocean: wind dependence and seasonal cycles, Atmos. Chem. Phys., 17, 4419-4432, 10.5194/acp-17-4419-2017, 2017.

Hong, S.-b., Yoon, Y. J., Becagli, S., Gim, Y., Chambers, S. D., Park, K.-T., Park, S.-J., Traversi, R., Severi, M., Vitale, V., Kim, J.-H., Jang, E., Crawford, J., and Griffiths, A. D.: Seasonality of aerosol chemical composition at King Sejong Station (Antarctic Peninsula) in 2013, Atmos. Environ., 223, 117185, https://doi.org/10.1016/j.atmosenv.2019.117185, 2020.

Hoppel, W. A., Fitzgerald, J. W., Frick, G. M., Larson, R. E., and Mack, E. J.: Aerosol size distributions and optical properties found in the marine boundary layer over the Atlantic Ocean, J. Geophys. Res., 95, 3659-3686, 10.1029/JD095iD04p03659, 1990.

Humphries, R. S., Schofield, R., Keywood, M. D., Ward, J., Pierce, J. R., Gionfriddo, C. M., Tate, M. T., Krabbenhoft, D. P., Galbally, I. E., Molloy, S. B., Klekociuk, A. R., Johnston, P. V., Kreher, K., Thomas, A. J., Robinson, A. D., Harris, N. R. P., Johnson, R.,

and Wilson, S. R.: Boundary layer new particle formation over East Antarctic sea ice – possible Hg-driven nucleation?, Atmos. Chem. Phys., 15, 13339-13364, 10.5194/acp-15-13339-2015, 2015.

Humphries, R. S., Klekociuk, A. R., Schofield, R., Keywood, M., Ward, J., and Wilson, S. R.: Unexpectedly high ultrafine aerosol concentrations above East Antarctic sea ice, Atmos. Chem. Phys., 16, 2185-2206, 10.5194/acp-16-2185-2016, 2016.

Humphries, R. S., McRobert, I. M., Ponsonby, W. A., Ward, J. P., Keywood, M. D., Loh, Z. M., Krummel, P. B., and Harnwell, J.: Identification of platform exhaust on the RV Investigator, Atmos. Meas. Tech., 12, 3019-3038, 10.5194/amt-12-3019-2019, 2019.

Humphries, R. S., Miljevic, B., Mallet, M., Keywood, M. D., Ward, J., Cravigan, L. T., Mace, G. G., Gribben, S., Protat, A., McRobert, I., Woodhouse, M. T. and Fiddes, S.: Changes in composition across the Antarctic atmospheric Polar Front, *in prep.*

Legrand, M., Yang, X., Preunkert, S., and Theys, N.: Year-round records of sea salt, gaseous, and particulate inorganic bromine in the atmospheric boundary layer at coastal (Dumont d'urville) and central (concordia) East Antarctic sites, J. Geophys. Res., 121, 997-1023, 10.1002/2015JD024066, 2016.

McGill, R., Tukey, J. W., and Larsen, W. A.: Variations of Box Plots, The American Statistician, 32, 12-16, 10.2307/2683468, 1978.

Myhre, G., D. Shindell, F.-M. Bréon, W. Collins, J. Fuglestvedt, J. Huang, D. Koch, J.-F. Lamarque, D. Lee, B. Mendoza, T. Nakajima, A. Robock, G. Stephens, T. Takemura, H. Zhang.: Anthropogenic and Natural Radiative Forcing., in: Climate Change 2013: The Physical Science Basis. Contribution of Working Group I to the Fifth Assessment Report of the Intergovernmental Panel on Climate Change, edited by: Stocker, T. F., D. Qin, G.-K. Plattner, M. Tignor, S.K. Allen,, and J. Boschung, A. N., Y. Xia, V. Bex, P.M. Midgley, Cambridge University Press, Cambridge, United Kingdom and New York, NY, USA., 2013.

Nylen, T. H., Fountain, A. G., and Doran, P. T.: Climatology of katabatic winds in the McMurdo dry valleys, southern Victoria Land, Antarctica, J. Geophys. Res.-Atmos., 109, 10.1029/2003jd003937, 2004.

Penner, J. E., Zhou, C., and Xu, L.: Consistent estimates from satellites and models for the first aerosol indirect forcing, Geophys. Res. Lett., 39, 10.1029/2012GL051870, 2012.

Pook, M.: The Roaring Forties sometimes purr. In: Australian Antarctic Magazine, 4, Australian Antarctic Division, Hobart, 2002.

Quinn, P. K., Coffman, D. J., Kapustin, V. N., Bates, T. S., and Covert, D. S.: Aerosol optical properties in the marine boundary layer during the First Aerosol Characterization Experiment (ACE 1) and the underlying chemical and physical aerosol properties, J. Geophys. Res.-Atmos., 103, 16547-16563, 10.1029/97jd02345, 1998.

R Core Team: R: A language and environmental for statisitical computing. R Foundation for Statistical Computing, Vienna, Austria, 2017.

Regayre, L. A., Schmale, J., Johnson, J. S., Tatzelt, C., Baccarini, A., Henning, S., Yoshioka, M., Stratmann, F., Gysel-Beer, M., Grosvenor, D. P., and Carslaw, K. S.: The value of remote marine aerosol measurements for constraining radiative forcing uncertainty, Atmos. Chem. Phys., 20, 10063-10072, 10.5194/acp-20-10063-2020, 2020.

Schmale, J., Baccarini, A., Thurnherr, I., Henning, S., Efraim, A., Regayre, L., Bolas, C., Hartmann, M., Welti, A., Lehtipalo, K., Aemisegger, F., Tatzelt, C., Landwehr, S., Modini, R. L., Tummon, F., Johnson, J., Harris, N., Schnaiter, M., Toffoli, A., Derkani, M., Bukowiecki, N., Stratmann, F., Dommen, J., Baltensperger, U., Wernli, H., Rosenfeld, D., Gysel-Beer, M., and Carslaw, K.: Overview of the Antarctic Circumnavigation Expedition: Study of Preindustrial-like Aerosols and Their Climate Effects (ACE-SPACE), B. Am. Meteorol. Soc., 100, 2260–2283, 10.1175/bams-d-18-0187.1, 2019.

Shindell, D. T., Lamarque, J. F., Schulz, M., Flanner, M., Jiao, C., Chin, M., Young, P. J., Lee, Y. H., Rotstayn, L., Mahowald, N., Milly, G., Faluvegi, G., Balkanski, Y., Collins, W. J., Conley, A. J., Dalsoren, S., Easter, R., Ghan, S., Horowitz, L., Liu, X., Myhre, G., Nagashima, T., Naik, V., Rumbold, S. T., Skeie, R., Sudo, K., Szopa, S., Takemura, T., Voulgarakis, A., Yoon, J. H., and Lo, F.: Radiative forcing in the ACCMIP historical and future climate simulations, Atmos. Chem. Phys., 13, 2939-2974, 10.5194/acp-13-2939-2013, 2013.

Whittlestone, S., and Zahorowski, W.: Baseline radon detectors for shipboard use: Development and deployment in the First Aerosol Characterization Experiment (ACE 1), J. Geophys. Res.-Atmos., 103, 16743-16751, doi:10.1029/98JD00687, 1998.

Yan, J., Jung, J., Lin, Q., Zhang, M., Xu, S., and Zhao, S.: Effect of sea ice retreat on marine aerosol emissions in the Southern Ocean, Antarctica, Sci. Total Environ., 745, 140773, https://doi.org/10.1016/j.scitotenv.2020.140773, 2020.